Nanoscale Advances

ROYAL SOCIETY OF CHEMISTRY

PAPER

View Article Online
View Journal | View Issue

Cite this: *Nanoscale Adv.*, 2023, **5**, 934

200 MPa cold isostatic pressing creates surface-microcracks in a Zn foil for scalable and long-life zinc anodes†

Di Zhang‡, Hongfei Lu‡, Nawei Lyu‡, Xin Jiang, Zili Zhang and Yang Jin *

The Zn anode suffers from severe dendrite growth and side reactions, which restrict its development in the realm of large-scale energy storage. Herein, in this study, we propose a method to create surface-microcracks in a Zn foil by 200 MPa cold isostatic pressing. The proposed pressing method can avoid the surface tip effect of Zn, and creates a subtly surface-microcracked zinc structure, providing more zinc ion transport channels, thereby effectively alleviating the dendrite growth and side reactions during the repeated Zn plating and stripping. Benefiting from these advantages, the 200 MPa Zn||Zn symmetric cell can achieve a long cycle life (1525 h) of 1 mA h cm^{-2} at 2 mA cm^{-2}. The 200 MPa Zn||VO_2 full cell can still maintain a capacity of 110 mA h g^{-1} after 1000 cycles at 0.1 A g^{-1}. In addition, assembled pouch cells also show excellent cycling stability. The proposed cold isostatic pressing method is compatible with large-scale production applications and provides an effective strategy for realizing high-performance zinc anodes for zinc-ion batteries.

Received 6th October 2022
Accepted 5th January 2023

DOI: 10.1039/d2na00682k

rsc.li/nanoscale-advances

1. Introduction

Aqueous zinc-ion batteries are considered promising candidates for renewable energy storage due to their safety, low toxicity, and high theoretical capacity (820 mA h g^{-1}).[1–3] In recent years, although researchers have achieved an obvious development of high-performance zinc-ion battery cathodes and electrolytes, the issue of Zn metal itself has been underestimated.[4,5] The inherent defects and uneven growth of zinc dendrites shorten the life of zinc-ion batteries.[6,7] At the same time, due to the presence of tips and impurities on the surface of mass-produced Zn foils, these regions are conducive to the nucleation of Zn ions during Zn deposition,[8,9] which leads to further deposition in subsequent cycles causing the dendrite growth.[10] Therefore, how to solve the problem of zinc dendrite growth is an important challenge.[11]

In order to solve this challenge of obtaining high-performance zinc anodes, the research procedure mainly involves the following ways to improve the performance of zinc anodes, (i) covering the zinc surface with a protective layer,[12–14] (ii) adjusting the structure of the electrolyte,[15–17] and (iii) changing the metal structure of the zinc anode.[18–20] Recently, it has been reported that creating a copper–zinc alloy material on the zinc surface inhibits the electrochemical corrosion of aqueous zinc metal and improves the cycle performance.[21] To guide the preferential deposition of zinc ions, the researcher prepared an $AgZn_3$ coating on the zinc metal surface by the plasma sputtering method;[22] others include Ag coating[23] and Zn–Sn alloy coating.[24,25] Coating a protective layer on the zinc surface can improve the cycle performance of zinc-ion batteries, but it has high requirements on the uniformity and thickness of the protective layer.[26–28] In addition, a study has shown that electrolyte additive is a simple and effective way to improve the performance of zinc-ion batteries.[29] For example, the performance of zinc-ion batteries was improved by adding a small amount of diethyl ether additive to the electrolyte of zinc-ion batteries;[30] the structure of the electrolyte was adjusted by the addition of tetrabutylammonium sulfate, thereby inducing uniform zinc deposition.[31] Adding electrolyte additives is a simple modification method, but these additives may destroy the original safety and economy of aqueous zinc batteries.[32] Therefore, from the perspective of industrialization, the above methods are difficult for mass production.[33,34]

It is effective to change the original structure of zinc to create a structure on the zinc surface.[35–37] For example, Zn–Cu alloys were prepared by combining the samples with the electrochemically assisted annealing thermal method.[38] The structured Zn–Cu alloys can provide high electron and ion transport paths for the uniform deposition of Zn.[39,40] Chen *et al.* reported a double porous Zn-3D@600 protective layer by coating a Zn@C zinc skeleton. This Zn-3D@600 anode exhibits high stability and low polarization voltage during the galvanization/stripping process. Li *et al.* reported a modification method for zinc anodes by utilizing a ball-milling clay precipitate (designated as

Research Center of Grid Energy Storage and Battery Application, School of Electrical Engineering, Zhengzhou University, Zhengzhou 450001, Henan, China. E-mail: yangjin@zzu.edu.cn

† Electronic supplementary information (ESI) available. See DOI: https://doi.org/10.1039/d2na00682k

‡ These authors contributed equally to this work.

BMC, consisting of the unetched MAX phase and the $Ti_3C_2T_x$ phase) to construct a three-dimensional (3D) framework on the surface of a zinc foil (Zn@BMC).[35] In addition, some researchers changed the structure of zinc metal by rolling from the problem of zinc metal itself,[41] and adjusted the preferential deposition of zinc crystal plane.[19,42] However, this method was developed by changing the zinc metal into a molten state at 500 °C, then cooling it to normal temperature, and repeatedly rolling it for 3 cycles to deform it. The structure is difficult to commercialize due to the complicated process and high cost.[18] Since the tensile strength of the Zn metal is about 110 MPa,[43] the surface microcrack structure cannot be achieved by simple rolling. Therefore, exploring simple and effective methods for improving the structure of zinc has high practical value for the rational design of zinc anodes.[44,45]

Herein, here, we propose a surface-microcracked Zn structure prepared by 200 MPa cold isostatic pressing. Cold isostatic pressing is a commonly used technology for the large-scale processing of metal structures (Fig. 1a). It is a simple physical treatment method and can be used to apply isobaric pressure to metals. It is proved that 200 MPa cold isostatic pressing can skillfully create zinc surface microcracks to achieve uniform deposition of Zn ions (Fig. 1b and S1†). These microcracks subtly create the Zn structure, which exposes more deposition of the sites. When the electrolyte is immersed inside the microcrack structure during deposition, it provides more zinc ion transport channels. These channels help regulate the uniform deposition of zinc ions, while effectively avoiding the "tip effect" during zinc production (Fig. 1d). However, due to the surface protrusions and impurities of pure zinc during the production process, the serious growth of dendrites affects the performance of the zinc anode (Fig. 1c). On the basis of these advantages, a long cycle life of over 1500 h for the 200 MPa Zn||Zn symmetric cell and super cycling stability of up to 1000 cycles for the 200 MPa Zn||VO_2 full cell was achieved. This work provides an effective strategy for large-scale improvement in the performance of the zinc anode.

2. Results and discussion

2.1. Analysis of the interface characteristics and mechanism of a zinc anode

Compared with previous studies, the outstanding features of this treatment method are (i) large-scale mass production and simple process, (ii) clever design of the surface-microcrack

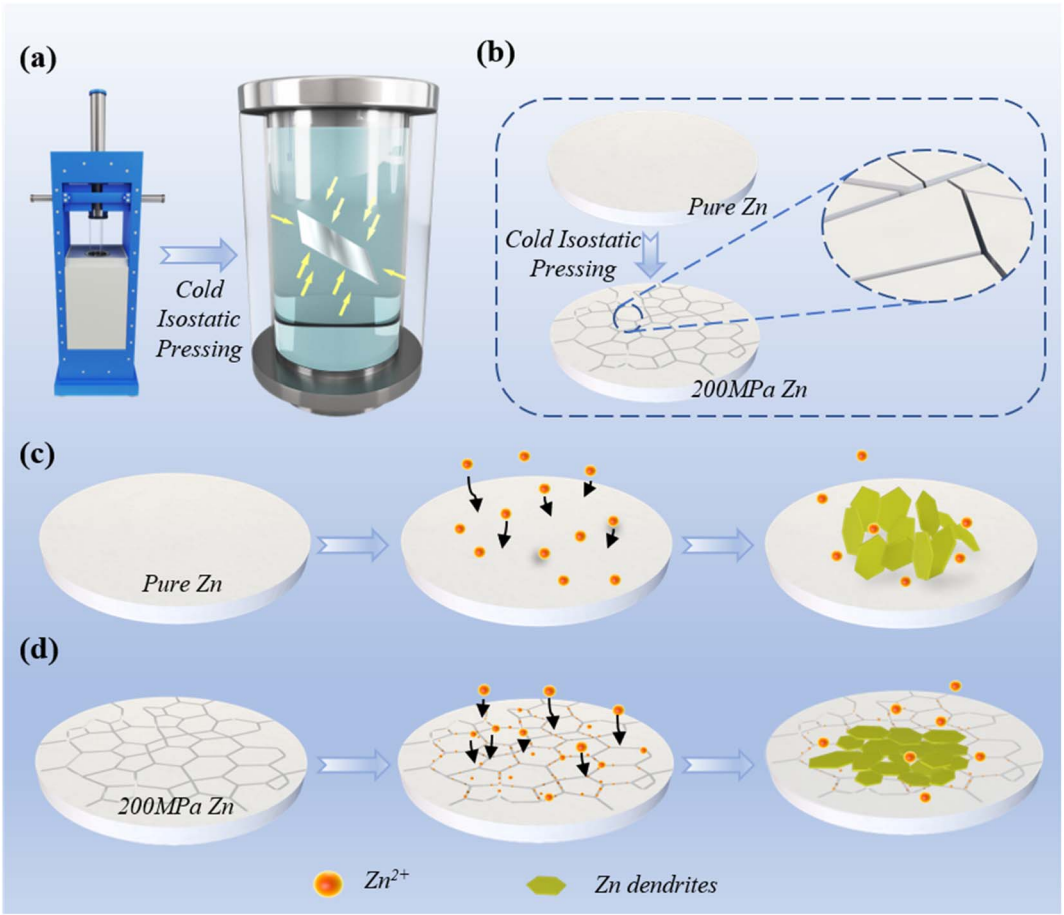

Fig. 1 Principle of cold isostatic pressing and schematic of zinc deposition. (a) Schematic of the principle of cold isostatic pressing of Zn: the zinc foil is subjected to isobaric treatment in all directions in the press chamber; (b) the schematic of the microcracks of the zinc surface created by cold isostatic pressing: the surface produces a structure of microcracks; (c) schematic of pure Zn deposition: disordered and uneven growth of dendrites; (d) schematic of 200 MPa Zn deposition: orderly and uniform growth of dendrites.

structure to increase zinc ion transport channels and (iii) stable performance and more practicality. Fig. 2a shows the surface changes of the zinc foil (1 m long, 30 μm thick) before and after cold isostatic pressing at 200 MPa. Before the treatment, the surface of the zinc foil is rough with many impurities and protrusions, while the surface becomes relatively smooth and flat with metallic luster and dark yellow after the treatment. In Fig. 2b, SEM images show that 200 MPa cold isostatic pressing pressure-treated zinc foil subtly formed various microcracks on the surface (Fig. S2a†). From the SEM image of pure zinc (Fig. 2c), it can be found that the zinc surface has uneven protrusions. Due to the inevitable defects and impurities in the production process, the surface roughness of pure zinc affects the cycle performance (Fig. 2c and S2b†).

Atomic force microscopy (AFM) images clearly showed various spikes on the surface of pure Zn, while the surface of 200 MPa Zn was relatively flat (Fig. 2c, d and S3†). This is related to the defects in zinc itself from the production process. Thermodynamically, the presence of dendrites favors the

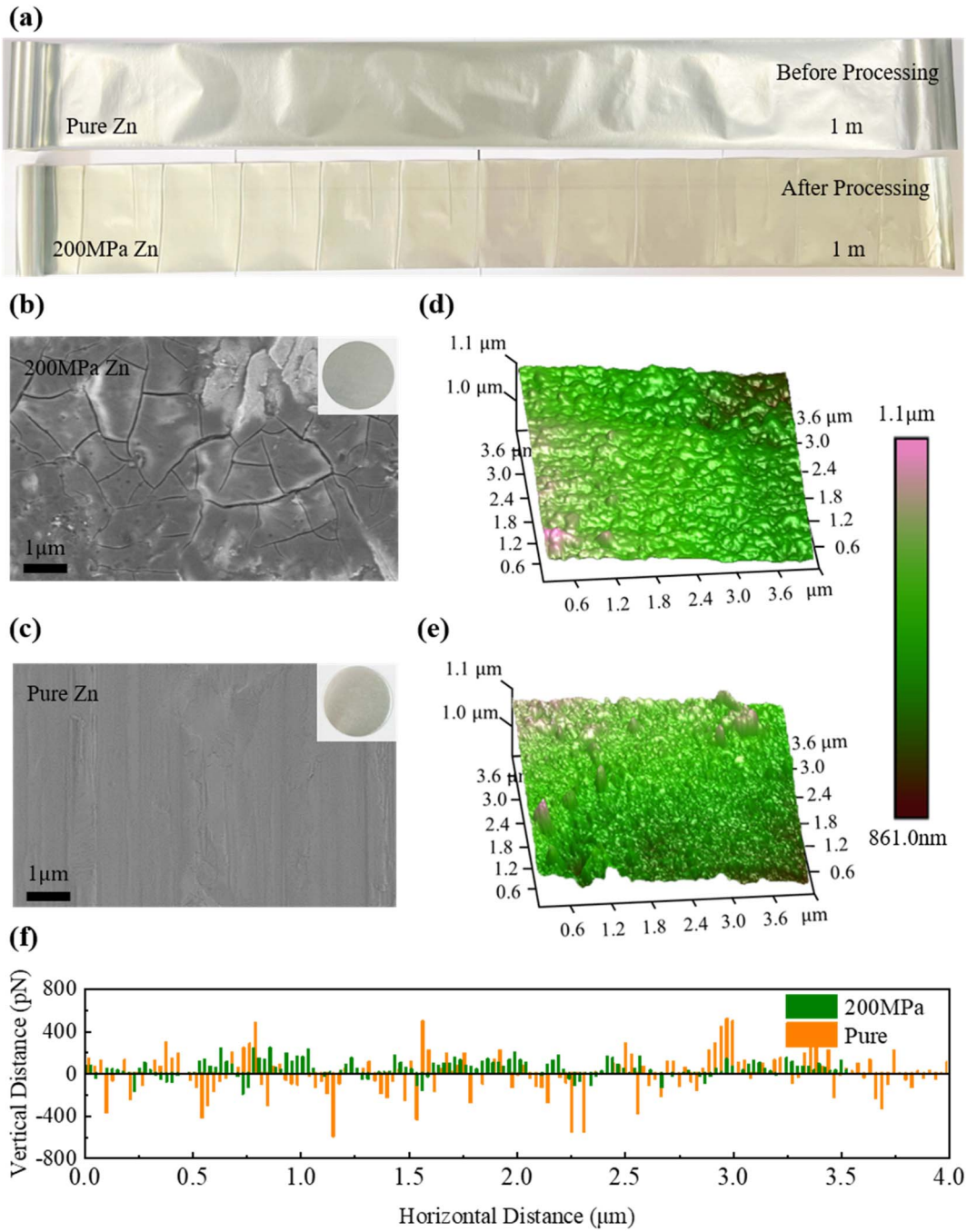

Fig. 2 Interface characteristics between pure Zn and 200 MPa Zn foil. (a) Photos of large-scale zinc foil before and after treatment; (b) SEM images of 200 MPa Zn and (c) pure Zn; (d) AFM images of 200 MPa Zn and (e) pure Zn; (f) 200 MPa Zn and pure Zn surface flatness curves.

preferential deposition of Zn^{2+}, resulting in a "tip effect". This promotes the deposition of zinc ions and eventually leads to the growth of dendrites that puncture the membrane. Therefore, the presence of dendrites directly limits the battery life. In Fig. 2f, by selecting the zinc surface topography in the 0–4 μm region, the changes in the degree of concavity and convexity on the zinc surface can be seen more intuitively (Fig. S7†). Compared with pure Zn, 200 MPa Zn avoids the growth of dendrites along the dendrite direction, which can improve the cycle stability of zinc-ion batteries.

2.2. Comparative analysis of different pressure treatments of cold isostatic pressing

In order to find out the influence of the pressure in the cold isostatic pressing process on the performance of the zinc anode, the zinc foil was subjected to isobaric treatment at 50 MPa, 100 MPa, 200 MPa, and 300 MPa. The pressure holding time (120 s) was the same. XRD data show that the (002) crystal face of 200 MPa zinc foil had an increasing trend, which is beneficial to the uniform and dense deposition of zinc ions (Fig. S4†). Raman data are shown in Fig. S5,† it was found that there were oxide peaks on the zinc surface. However, the 200 MPa Zn oxide peak intensity was relatively small, indicating that there were relatively few impurity defects on the 200 MPa Zn surface. This is because the 200 MPa pressure could remove the oxide layer from the zinc surface.

To visualize the mechanism of Zn surface dendrites, a schematic of Zn dendrite growth is presented here. As shown in Fig. 3a, due to the lack of any treatment on the surface of pure Zn, the impurities on the surface and the dendrite phenomenon lead to the disordered and uneven growth of dendrites. The cold isostatic pressing process flattens the defects and impurities on the surface of Zn, and the created microcrack structures will induce zinc ions in the surface (Fig. 3b). The surface is uniformly deposited, thereby increasing its cycling stability. After cycling, they were disassembled to observe the growth morphology of dendrites on the zinc surface (Fig. 3c–f, S6 and S12†). The results show that the effect of different pressure

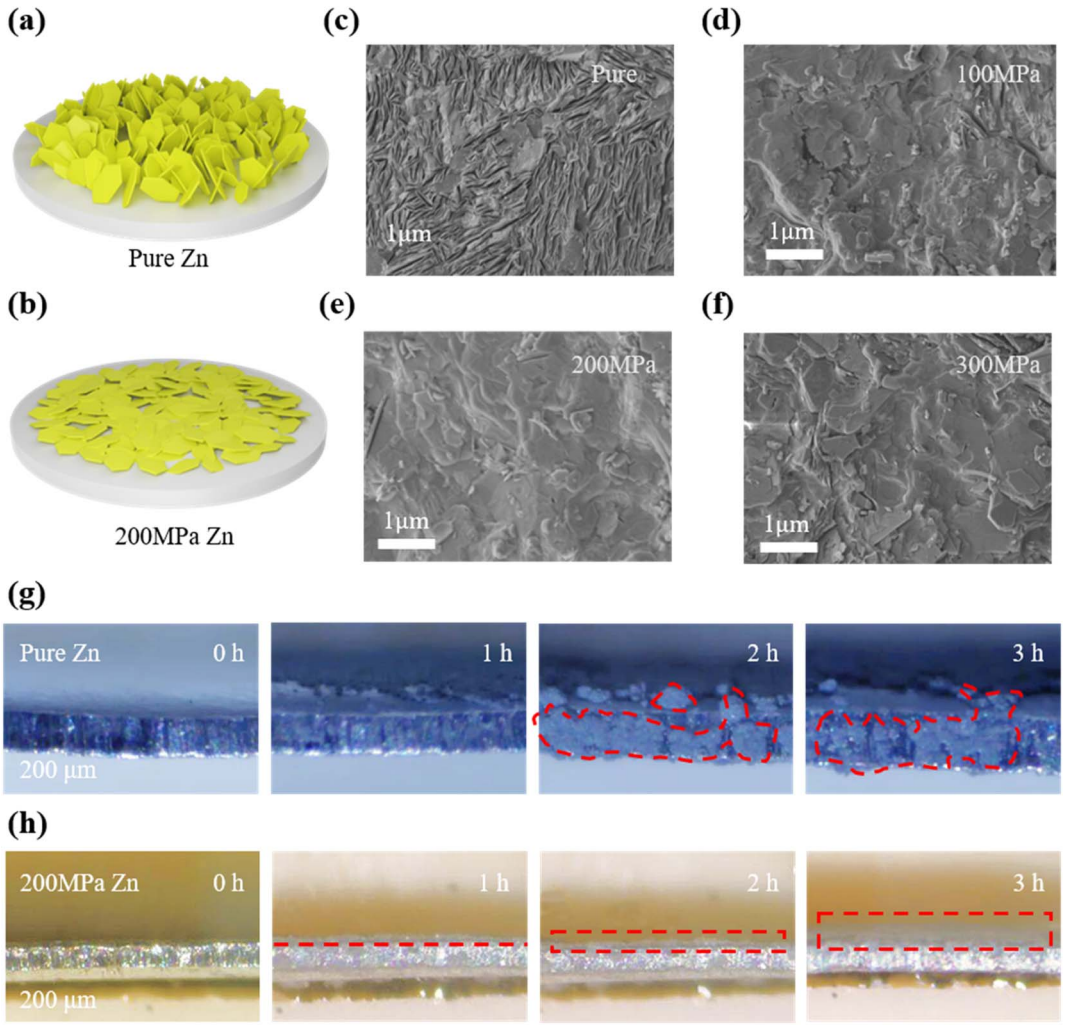

Fig. 3 Zinc anode nucleation mechanism. (a) Schematic of Zn dendrite growth of pure Zn and (b) 200 MPa Zn: (a) disordered heterogeneous growth; (b) ordered horizontally uniform growth; c) pure Zn, (d) 100 MPa Zn, (e) 200 MPa Zn and (f) 300 MPa Zn surface dendrites SEM images of growth; (g) pure Zn and (h) 200 MPa Zn *in situ* observation images: (g) disordered growth of larger dendrites; (h) flocculent ordered growth.

treatments is far more uniform than that of pure Zn. The most obvious is 200 MPa Zn, in which the zinc deposition is dense and uniform (Fig. 3e and S13†).

Through the *in situ* optical observations on pure Zn and 200 MPa Zn anodes, it can be intuitively found that several large dendrites grow disorderly on the pure Zn anode (Fig. 3g). The dendrites appeared in 1 hour, and the dendrites grew obviously in 2 hours. After 3 hours, the dendrites agglomerated and grew into larger particles. There are no large dendrites on the surface of the 200 MPa Zn anode, but flocculent growth was observed (Fig. 3h). Zinc ions are deposited densely and uniformly on the zinc surface. This is attributed to the microcracks inside zinc, which provide more transport channels for the zinc ions, inducing a uniform deposition of the zinc ions.

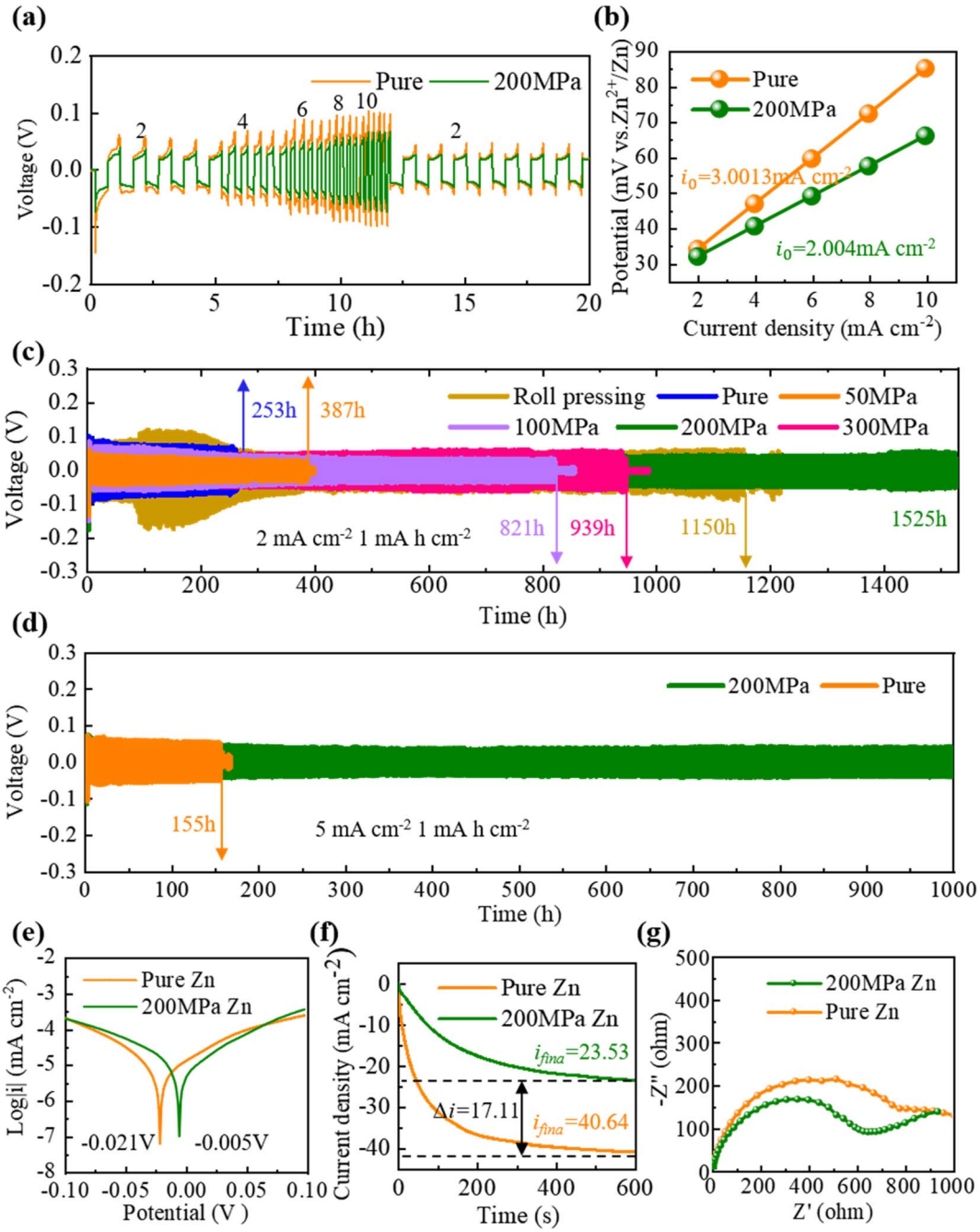

Fig. 4 Electrochemical performance of symmetrical cells. (a) The rate capability of pure Zn and 200 MPa Zn; (b) the exchange current density fitting curves of pure Zn and 200 MPa Zn; (c) long cycle results of zinc foil treated with different pressures such as pure, 50 MPa, 100 MPa, 200 MPa, 300 MPa and ross pressing under the conditions of 2 mA cm^{-2} and 1 mA h cm^{-2}; (d) long cycle results of pure Zn and 200 MPa Zn under the conditions of 5 mA cm^{-2} and 1 mA h cm^{-2}; comparison of (e) Tafel curves, (f) CA curves and (g) EIS curves between pure Zn and 200 MPa Zn symmetric cells.

2.3. Analysis of the electrochemical performance of symmetrical batteries

In order to accurately evaluate the kinetic performance of the deposited Zn ions, the rate performance of the symmetric cells was tested at 2 to 10 mA cm^{-2} (Fig. 4a and S10†). 200 Mpa Zn has a smaller overpotential than pure Zn. In order to further intuitively describe the deposition process of Zn, the exchange current density of zinc-ion battery deposition is calculated by fitting the rate capability and the following formula:[22,46]

$$i_0 = \frac{RT}{zF\eta} i$$

Where i_0 is the exchange current density; I is the current density; η is total overpotential; R is the gas constant; T is the thermodynamic temperature; F is the Faraday constant; z is the number of electrons involved in the electrode reaction.

The fitting result of the calculated data is shown in Fig. 4b (Table S1†). The exchange current density of the 200 mPa zinc-ion battery is 2.004 mA cm^{-2}, which is lower than that of pure Zn (3.0013 mA cm^{-2}). This shows that 200 mPa Zn has a small overpotential and good zinc ion deposition kinetics.[46]

The excellent long cycle life of the symmetric cell directly reflects the effectiveness of the cold isostatic pressing 200 mPa Zn treatment (Fig. 4c and d). In Fig. 4c, the Zn||Zn symmetric cells are assembled from pure, 50 mPa, 100 mPa, 200 mPa, and 300 mPa Zn foil under the conditions of 2 mA cm^{-2} and 1 mA h cm^{-2}. At the same time, the cell cycle performance and roll pressure were compared with those reported previously. The results show that 100 mPa, 200 mPa, and 300 mPa showed good electrochemical performance, of which, 200 MPa had the most obvious effect. The cycle life of the 200 MPa Zn||Zn symmetrical cell (2 mA cm^{-2},1 mA h cm^{-2}) reaches 1525 h, approximately 7 times longer than that of pure Zn (Fig. S15†). The EDS images of the dead 200 MPa and pure Zn cells showed that 200 MPa Zn is uniformly deposited on the surface (Fig. S6†). In addition, the cycle performance of the symmetric

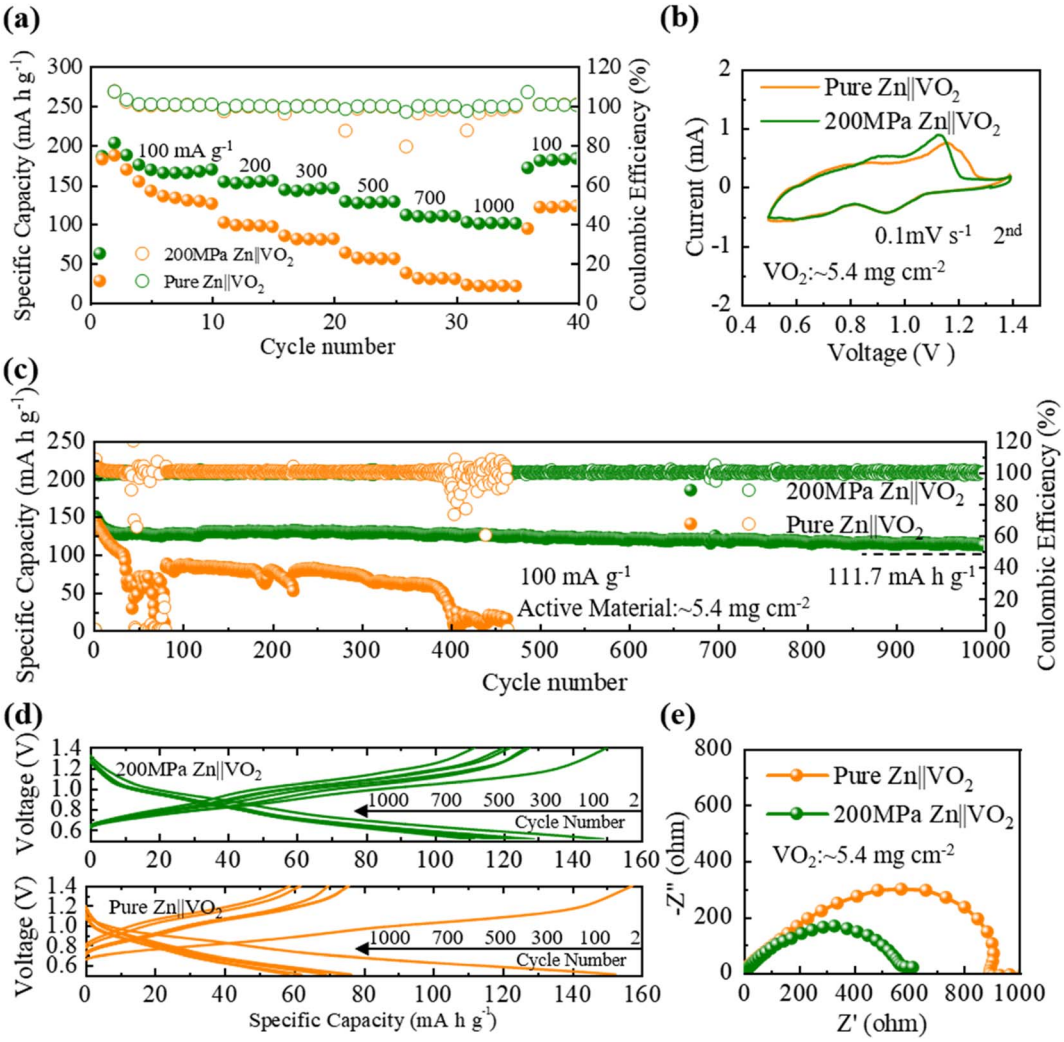

Fig. 5 Electrochemical performance of full cells. (a) 200 Mpa Zn||VO_2 and pure Zn||VO_2 full cells rate performance; (b) CV test curves: compare the full cell CV performance of the same active mass material at a scan rate of 0.1 mV s^{-1}; (c) discharge specific capacity and cycle efficiency of 200 Mpa Zn||VO_2 and pure Zn||VO_2 full cells at 100 mA g^{-1}; (d) comparison of specific capacity and voltage plateau curves of full cells under different cycling number; (e) EIS curves of 200 Mpa Zn||VO_2 and pure Zn||VO_2 full cells.

cell at high current densities of 5 mA cm^{-2} and 1 mA h cm^{-2} was tested (Fig. 4d and S8†). It was found that the cycle life of 200 MPa Zn can reach more than 1000 h, far exceeding that of pure Zn (155 h).

Since the corrosion behavior and side reactions in Zn-ion batteries are closely related, the linear polarization curves of the batteries assembled with pure Zn and 200 MPa Zn were investigated, as shown in Fig. 4e. The results show that the 200 MPa Zn anode has a higher positive corrosion potential, indicating an improved chemical stability and corrosion inhibition rate of 200 MPa Zn relative to pure Zn. Then, chronoamperometry (CA) characterization was performed on the pure Zn and 200 MPa Zn assembled symmetric cells to further verify the zinc ion deposition behavior (Fig. 4f). The change in the current density of the CA curves can directly reflect the change in the zinc surface morphology. The difference between the initial current and the final current values indicates the degree of increase of the active area, which can reflect the growth of zinc ions. The final current of pure Zn is 40.64 mA cm^{-2} and 23.53 mA cm^{-2} for 200 Mpa Zn. The difference between the two is 17.11 mA cm^{-2}, which indicates that pure Zn has faster ion and electron transfer rates and it is easier to grow dendrites on the surface crystal. The EIS curve reflects the hindrance of ion and electron migration in the cell.[47,48] The EIS curves of symmetric cells were also tested (as shown in Fig. 4g), verifying that the R_{ct} values of 200 MPa Zn were much lower than those of pure Zn. 200 MPa Zn has a significantly reduced impedance relative to pure Zn, reflecting excellent electrochemical performance.

2.4. Analysis of the electrochemical performance of full batteries

To verify the effectiveness of 200 MPa Zn in the electrochemical performance of the full cell, here, the Zn||VO_2 full cell was assembled with VO_2 as the cathode. The cathode was produced by the rolling sheet method. The loading of VO_2 active material was about 5.4 mg cm^{-2}. First, the rate performance of 200 MPa Zn||VO_2 and pure Zn||VO_2 full cells was tested. As shown in Fig. 5a, 200 MPa Zn exhibited excellent

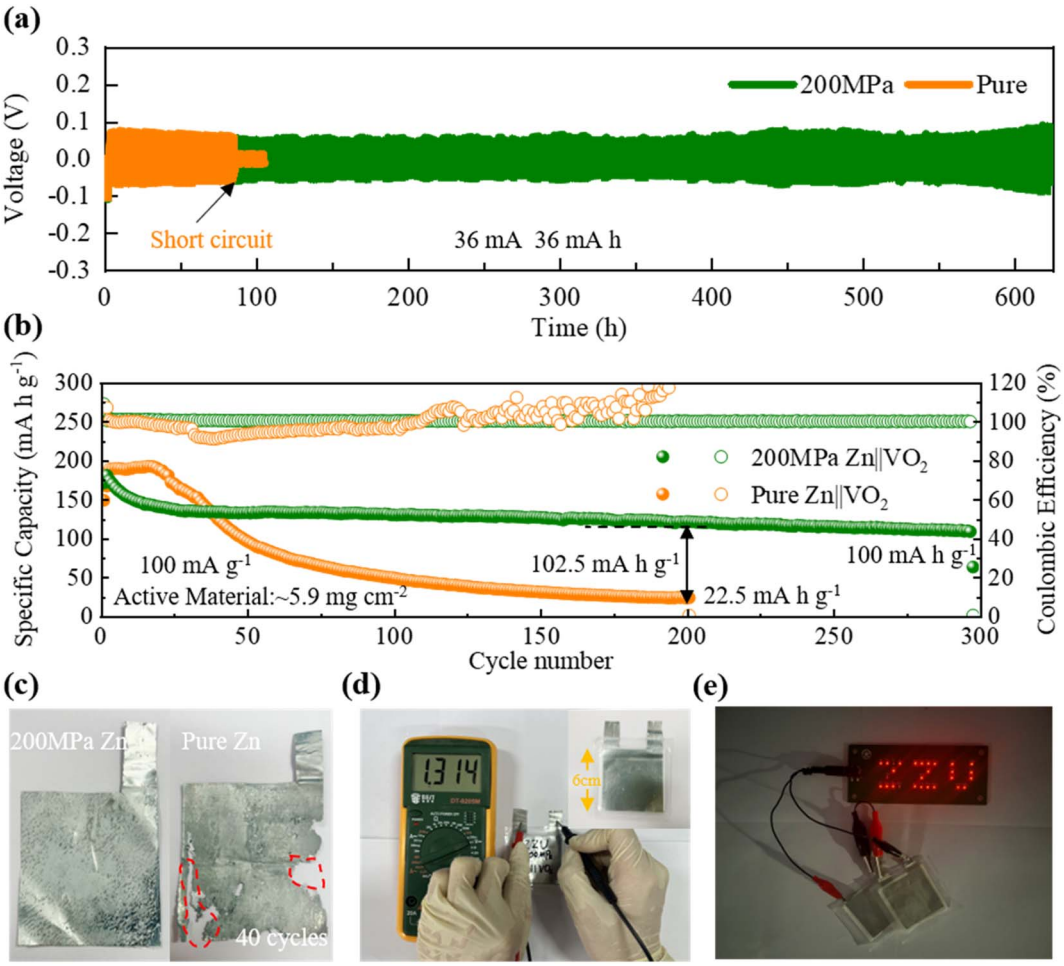

Fig. 6 Electrochemical performance of pouch cells. (a) The long–term cycle performance of the pouch symmetric cell at 36 mA and 36 mA h; (b) the electrochemical performance of the pouch full cells with the active material controlled at ≈ 5.9 mg cm^{-2} under the condition of 0.1 A g^{-1}; (c) surface morphologies of zinc electrodes in pouch symmetrical cells after 40 cycles; (d) 200 MPa Zn||VO_2 pouch full cell and open circuit voltage; (e) 200 MPa Zn||VO_2 pouch full cell lighting LEDs.

performance when the current density was from 100 to 1000 mA g^{-1}. The results show that the rate performance of the 200 MPa Zn full cell is significantly better than that of pure Zn, showing excellent capacity retention. Then, at a scan rate of 0.1 mV s^{-1}, the cyclic voltammetry (CV) test results of the full cell also confirmed that 200 MPa Zn could promote the electrode reaction (Fig. 5b).

As shown in Fig. 5c, the active material quality of the full cell is controlled at $\approx$ 5.4 mg cm^{-2}. After 1000 cycles, the specific capacity of the 200 MPa Zn‖VO_2 full battery remains above 110 mA h g^{-1}, while the pure Zn‖VO_2 full cell is shorted at 400 cycles, and the capacity decays rapidly. Furthermore, when the cycle number increases from 100 to 1000 cycles, the 200 MPa Zn‖VO_2 full cell exhibited higher capacity retention and smaller polarization compared with pure Zn cells (Fig. 5d). From the EIS measurements, it can be found that the 200 MPa Zn‖VO_2 full cell has lower impedance and excellent electrochemical performance compared to pure Zn (Fig. 5e).

2.5. Analysis of the electrochemical performance of pouch batteries

In order to verify the validity and practicability of the 200 MPa cold isostatic pressings, further explanation is provided here through pouch batteries. 200 MPa Zn and pure Zn foils were assembled as 6 × 6 cm Zn‖Zn pouch symmetric cells, and the 200 MPa Zn pouch symmetric cell achieved a long cycle life (over 650 h) at 36 mA h (Fig. 6a and S9†). As the zinc foil area of the pouch battery is larger, it is more prone to short-circuit death than the button battery. This is because zinc dendrites can grow anywhere, pierce the separator, and cause short circuits. The symmetric cell life of the pouch assembled with 200 MPa Zn can be as long as more than 650 h, while that of the pure Zn pouch cell is short-circuited in only 84 h. When the electrode was disassembled to observe the deposition on the zinc surface, it can be found that pure zinc nucleated locally and had large dendrites, while 200 MPa Zn nucleated uniformly, with a dense surface and good nucleation morphology.

In Fig. 6b, the pouch full cells assembled with an active material of $\approx$ 5.9 mg cm^{-2}. After 300 cycles, the 200 MPa Zn‖VO_2 cell had a capacity of 100 mA h g^{-1} with 80% retention, while the pure zinc cell capacity decayed rapidly and died after 200 cycles. It can be seen that 200 MPa Zn showed an extremely high practical value.

The pouch symmetric cell was disassembled after 40 cycles at 36 mA and 36 mA h, and the surface morphology of the zinc anode was observed (Fig. 6c). There is no obvious dendrite growth on the surface of 200 MPa Zn, while the surface of pure Zn is decayed and has obvious dendrites. The 200 MPa Zn‖VO_2 pouch full cell was 6 cm × 6 cm with an open circuit voltage of 1.314 V (Fig. 6d). It could successfully light LEDs (0.06 W/pc) to demonstrate their effectiveness (Fig. 6e). To evaluate its safety against external influences, piercing and cutting experiments were performed on the pouch cells here (Fig. S11†). The pouch cells can still work normally by piercing or cutting, thus proving the excellent safety and practicability of 200 MPa Zn pouch cells in practical applications.

3. Conclusions

Large-scale processing of zinc foil by 200 MPa cold isostatic pressing can ingeniously create a microcracked structure, which can provide more transfer channels for zinc ions. Due to the existence of surface microcracks, the obvious tip dendrite effect is avoided during the deposition process, enabling a long cycle life for the uniform deposition of zinc ions. The data of symmetric cells show that the 200 MPa Zn can achieve an excellent electrochemical performance of up to 1525 h, far exceeding that of pure Zn batteries. At the same time, the surface of the zinc anode after cycling is dense and uniform. More importantly, the capacity of the 200 MPa Zn‖VO_2 cell remains above 110 mA h g^{-1} after 1000 cycles, while the pure Zn cell decays rapidly, with only 400 cycles of short circuit and almost zero capacity decay. After 300 cycles of the pouch full cell, the specific capacity of 200 MPa Zn is 102 mA h g^{-1} higher than that of pure Zn, showing excellent cycle performance and a low decay rate. Therefore, the 200 MPa cold isostatic pressing strategy provides a new way for fundamental improvement and large-scale production of zinc anodes for zinc-ion batteries.

Author contributions

Di Zhang: methodology, investigation, data curation, formal analysis, writing – original draft. Hongfei Lu: methodology, investigation, data curation, formal analysis, writing – original draft. Nawei Lyu: investigation, validation. Xin Jiang: formal analysis, writing review & editing. Zili Zhang: methodology, investigation, data curation. Yang Jin: conceptualization, writing – review & editing, supervision, Funding acquisition.

Conflicts of interest

The authors declare no competing financial interest.

Acknowledgements

This work is supported by the National Natural Science Foundation of China (Grant Nos. 52177223) and the Postgraduate Education Reform and Quality Improvement Project of Henan Province (YJS2021JD02).

References

1 Z. Yang, Q. Zhang, C. Xie, Y. Li, W. Li, T. Wu, Y. Tang and H. Wang, *Energy Storage Mater.*, 2022, **47**, 319–326.
2 X. Zhang, J. P. Hu, N. Fu, W. B. Zhou, B. Liu, Q. Deng and X. W. J. I. Wu, *InfoMat*, 2022, e12306.
3 M. Erdiwansyah, H. Husin, M. Z. Nasaruddin and A. Muhibbuddin, *Prot. Control Mod. Power Syst.*, 2021, **6**, 37–54.
4 C. Yuan, L. Yin, P. Du, Y. Yu, K. Zhang, X. Ren, X. Zhan and S. Gao, *Chem. Eng. J.*, 2022, 442.
5 C. Li, X. Xie, H. Liu, P. Wang, C. Deng, B. Lu, J. Zhou and S. Liang, *Nat. Sci. Rev.*, 2022, **9**, nwab177.

6 J. Yang, B. Yin, Y. Sun, H. Pan, W. Sun, B. Jia, S. Zhang and T. Ma, *Nano-Micro Lett.*, 2022, **14**, 1–47.
7 Y. Bai, H. Zhang, M. Usman Tahir and B. Xiang, *J. Colloid Interface Sci.*, 2022, **608**, 22–29.
8 B.-F. Cui, X.-P. Han and W.-B. Hu, *Small Struct.*, 2021, **2**, 2000128.
9 H. Jia, Z. Wang, B. Tawiah, Y. Wang, C.-Y. Chan, B. Fei and F. J. N. E. Pan, *Nano Energy*, 2020, **70**, 104523.
10 G. Qian, G. Zan, J. Li, S. J. Lee, Y. Wang, Y. Zhu, S. Gul, D. J. Vine, S. Lewis and W. Yun, *Adv. Energy Mater.*, 2022, **12**, 2200255.
11 Y. Guo, *Prot. Control Mod. Power Syst.*, 2022, **7**, 602–618.
12 J. Ming, J. Guo, C. Xia, W. Wang and H. N. Alshareef, *Mater. Sci. Eng. R Rep.*, 2019, **135**, 58–84.
13 T. C. Li, Y. V. Lim, X. Xie, X. L. Li, G. Li, D. Fang, Y. Li, Y. S. Ang, L. K. Ang and H. Y. Yang, *Small*, 2021, **17**, e2101728.
14 M. Idrees, S. Batool, J. Cao, M. S. Javed, S. Xiong, C. Liu and Z. Chen, *Nano Energy*, 2022, **100**, 107505.
15 Y. Wang, Z. Wang, F. Yang, S. Liu, S. Zhang, J. Mao and Z. Guo, *Small*, 2022, 2107033.
16 J. Xu, W. Lv, W. Yang, Y. Jin, Q. Jin, B. Sun, Z. Zhang, T. Wang, L. Zheng and X. J. A. n. Shi, *ACS Nano*, 2022, **16**(7), 11392–11404.
17 Y. Quan, W. Zhou, T. Wu, M. Chen, X. Han, Q. Tian, J. Xu and J. Chen, *Chem. Eng. J.*, 2022, 446.
18 N. Guo, W. Huo, X. Dong, Z. Sun, Y. Lu, X. Wu, L. Dai, L. Wang, H. Lin and H. Liu, *Small Methods*, 2022, 2200597.
19 M. Zhou, S. Guo, J. Li, X. Luo, Z. Liu, T. Zhang, X. Cao, M. Long, B. Lu, A. Pan, G. Fang, J. Zhou and S. Liang, *Adv. Mater.*, 2021, **33**, e2100187.
20 X. Zhu, H. Zhang, Z. Wang, C. Zhang, L. Qin, D. Chen, S. Sun, C. Liu and J. Chen, *Mater. Today Energy*, 2022, **23**, 100897.
21 C. Li, X. Shi, S. Liang, X. Ma, M. Han, X. Wu and J. Zhou, *Chem. Eng. J.*, 2020, 379.
22 H. Lu, Q. Jin, X. Jiang, Z. M. Dang, D. Zhang and Y. Jin, *Small*, 2022, **18**, e2200131.
23 Q. Lu, C. Liu, Y. Du, X. Wang, L. Ding, A. Omar and D. Mikhailova, *ACS Appl. Mater. Interfaces*, 2021, **13**, 16869–16875.
24 Z. Liu, J. Ren, F. Wang, X. Liu, Q. Zhang, J. Liu, P. Kaghazchi, D. Ma, Z. Chi and L. Wang, *ACS Appl. Mater. Interfaces*, 2021, **13**, 27085–27095.
25 Z. Miao, M. Du, H. Li, F. Zhang, H. Jiang, Y. Sang, Q. Li, H. Liu and S. Wang, *EcoMat*, 2021, 3.
26 Y. Liu, T. Guo, Q. Liu, F. Xiong, M. Huang, Y. An, J. Wang, Q. An, C. Liu and L. Mai, *Mater. Today Energy*, 2022, **28**, 101056.
27 Z. Yi, G. Chen, F. Hou, L. Wang and J. J. A. E. M. Liang, *Adv. Energy Mater.*, 2021, **11**, 2003065.
28 Z. Cao, P. Zhuang, X. Zhang, M. Ye, J. Shen and P. M. Ajayan, *Adv. Energy Mater.*, 2020, **10**, 2001599.
29 T. Zhang, Y. Tang, S. Guo, X. Cao, A. Pan, G. Fang, J. Zhou and S. Liang, *Energy Environ. Sci.*, 2020, **13**, 4625–4665.
30 W. Xu, K. Zhao, W. Huo, Y. Wang, G. Yao, X. Gu, H. Cheng, L. Mai, C. Hu and X. Wang, *Nano Energy*, 2019, **62**, 275–281.
31 A. Bayaguud, X. Luo, Y. Fu and C. Zhu, *ACS Energy Lett.*, 2020, **5**, 3012–3020.
32 H. Dong, J. Li, J. Guo, F. Lai, F. Zhao, Y. Jiao, D. J. Brett, T. Liu, G. He and I. P. Parkin, *Adv. Mater.*, 2021, **33**, 2007548.
33 Y. Gao, Q. Cao, J. Pu, X. Zhao, G. Fu, J. Chen, Y. Wang and C. Guan, *Adv. Mater.*, 2022, 2207573.
34 J. Hao, B. Li, X. Li, X. Zeng, S. Zhang, F. Yang, S. Liu, D. Li, C. Wu and Z. Guo, *Adv. Mater.*, 2020, **32**, 2003021.
35 Y. M. Li, W. H. Li, W. Y. Diao, F. Y. Tao, X. L. Wu, X. Y. Zhang and J. P. Zhang, *ACS Appl. Mater. Interfaces*, 2022, **14**(20), 23558–23569.
36 C. Li, X. Shi, S. Liang, X. Ma, M. Han, X. Wu and J. Zhou, *Chem. Eng. J.*, 2020, **379**, 122248.
37 W. Li, Q. Zhang, Z. Yang, H. Ji, T. Wu, H. Wang, Z. Cai, C. Xie, Y. Li and H. Wang, *Small*, 2022, 2205667.
38 B. Liu, S. Wang, Z. Wang, H. Lei, Z. Chen and W. Mai, *Small*, 2020, **16**, e2001323.
39 K. Chen, H. Guo, W. Li and Y. Wang, *ACS Appl. Mater. Interfaces*, 2021, **13**, 54990–54996.
40 P. Cao, J. Tang, A. Wei, Q. Bai, Q. Meng, S. Fan, H. Ye, Y. Zhou, X. Zhou and J. Yang, *ACS Appl. Mater. Interfaces*, 2021, **13**, 48855–48864.
41 M. Zhou, S. Guo, J. Li, X. Luo, Z. Liu, T. Zhang, X. Cao, M. Long, B. Lu and A. Pan, *Adv. Mater.*, 2021, **33**, 2100187.
42 Z. Zhang, B. Xi, X. Ma, W. Chen, J. Feng and S. Xiong, *SusMat*, 2022, **2**, 114–141.
43 Y. Qin, P. Wen, D. Xia, H. Guo, M. Voshage, L. Jauer, Y. Zheng, J. H. Schleifenbaum and Y. Tian, *Adv. Mater.*, 2020, **33**, 101134.
44 W. Zhang, Y. Dai, R. Chen, Z. Xu, J. Li, W. Zong, H. Li, Z. Li, Z. Zhang and J. Zhu, *Angew. Chem., Int. Ed.*, 2022, e202212695.
45 J. Zheng, G. Zhu, X. Liu, H. Xie, Y. Lin, Y. Zeng, Y. Zhang, A. N. Gandi, Z. Qi and Z. Wang, *ACS Energy Lett.*, 2022, **7**, 4443–4450.
46 X. Xie, S. Liang, J. Gao, S. Guo, J. Guo, C. Wang, G. Xu, X. Wu, G. Chen and J. Zhou, *Energy Environ. Sci.*, 2020, **13**, 503–510.
47 W. Zong, H. Guo, Y. Ouyang, L. Mo, C. Zhou, G. Chao, J. Hofkens, Y. Xu, W. Wang and Y. E. Miao, *Adv. Funct. Mater.*, 2022, **32**, 2110016.
48 W. Zong, N. Chui, Z. Tian, Y. Li, C. Yang, D. Rao, W. Wang, J. Huang, J. Wang and F. Lai, *Adv. Sci.*, 2021, **8**, 2004142.